

# An accurate and flexible analog emulation of AdEx neuron dynamics in silicon

Sebastian Billaudelle<sup>†\*</sup>, Johannes Weis<sup>†</sup>, Philipp Dauer<sup>†</sup>, Johannes Schemmel<sup>†</sup>, *Member, IEEE*

\*sebastian.billaudelle@kip.uni-heidelberg.de <sup>†</sup>Kirchhoff-Institute for Physics, Heidelberg University, Germany

**Abstract**—Analog neuromorphic hardware promises fast brain emulation on the one hand and an efficient implementation of novel, brain-inspired computing paradigms on the other. Bridging this spectrum requires flexibly configurable circuits with reliable and reproducible dynamics fostered by an accurate implementation of the targeted neuron and synapse models. This manuscript presents the analog neuron circuits of the mixed-signal accelerated neuromorphic system BrainScaleS-2. They are capable of flexibly and accurately emulating the adaptive exponential leaky integrate-and-fire (AdEx) model equations in combination with both current- and conductance-based synapses, as demonstrated by precisely replicating a wide range of complex neuronal dynamics and firing patterns.

**Index Terms**—analog neuromorphic, AdEx, silicon neuron

## I. INTRODUCTION

**S**PIKING neuron models attempt to replicate the time-continuous dynamics and the event-based, asynchronous communication scheme of their archetype. Building on the simpler leaky integrate-and-fire (LIF) equation, the AdEx model captures these fundamental properties and can reproduce many of the dynamics and firing patterns found in electrophysiological recordings of biological neurons [1]. It describes the dynamics of the membrane potential  $V$  as

$$C \frac{dV}{dt} = -g_l (V - E_l) + g_l \Delta_T e^{\frac{V - V_T}{\Delta_T}} - w + I, \quad (1)$$

with membrane capacitance  $C$ , leak potential  $E_l$ , leak conductance  $g_l$ , soft threshold  $V_T$ , and exponential slope  $\Delta_T$ . The dynamics of the adaptation current  $w$  are governed by

$$\tau_w \frac{dw}{dt} = a (V - E_l) - w, \quad (2)$$

with time constant  $\tau_w$  and subthreshold adaptation strength  $a$ . The time-continuous dynamics are accompanied by spike-triggered jump conditions  $V \rightarrow V_r$  and  $w \rightarrow w + b$ .

Synaptic interaction is typically modeled by weighting and accumulating the presynaptic spike trains of each synapse  $i$ ,  $S_i(t) = \sum_j \delta(t - t_j)$ , and by convolving them with an interaction kernel, typically an exponential decay  $s(t) = \sum_i w_i S_i(t) \otimes \exp(t/\tau_{\text{syn}})$ . This integrator trace is then translated into a current onto the membrane either directly (*current-based*) or by modulating a conductance pulling the membrane towards a synaptic reversal potential (*conductance-based*):

$$I_{\text{cuba}} = \hat{I} \cdot s(t), \quad \text{or} \quad I_{\text{coba}} = \hat{g} \cdot s(t) \cdot [E_{\text{syn}} - V]. \quad (3)$$

The AdEx equations and other complex neuron models have inspired a plethora of analog neuromorphic implementations [2]–[6] and also lay the foundation for the silicon neuron presented in this manuscript. The discussed silicon neuron can accurately reproduce the original model dynamics and can be configured for a wide range of parameterizations.

The neuron circuits represent one of the central components of the analog core of BrainScaleS-2 (Fig. 1 A), a mixed-signal neuromorphic system emulating neuronal and synaptic dynamics on 1000-fold accelerated time scales compared to the biological nervous system. The silicon neurons are embedded into the rich infrastructure provided by the neuromorphic ASIC (Fig. 1 B). They receive weighted stimuli via the synapse array and relay their output spikes to the chip-internal event routing fabric. While partially controlled and interfaced through full-custom digital backend logic (Fig. 1 C), the neuronal dynamics are realized by analog circuits.

## II. SILICON IMPLEMENTATION

The design can be separated into multiple functional blocks mainly corresponding to the individual terms of the model equations. The circuit is implemented in a 65 nm bulk comple-

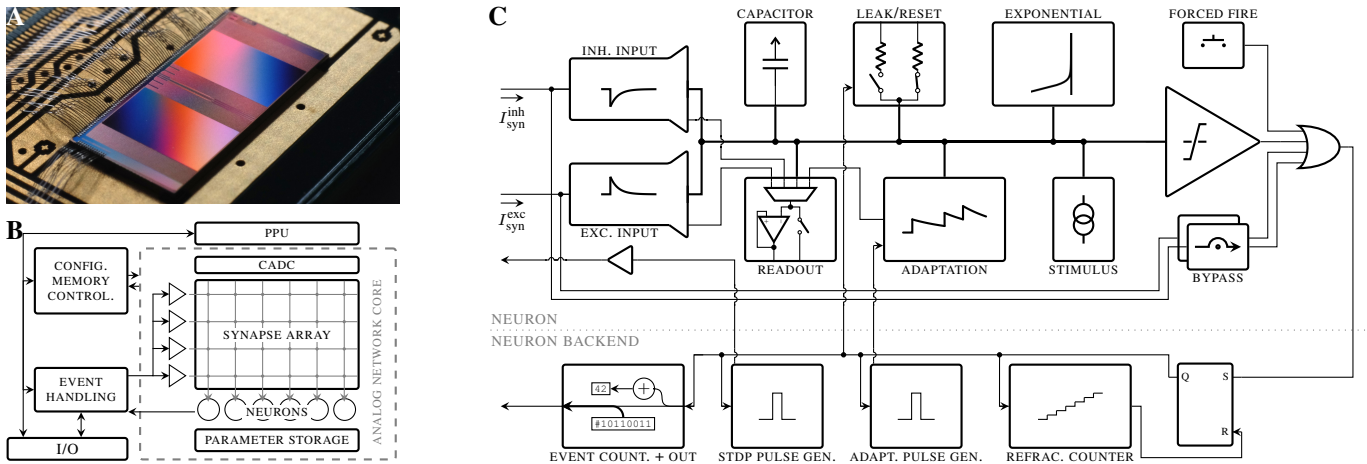


Fig. 1. (A) Photograph of a BrainScaleS-2 ASIC. (B) Block-level schematic of the neuromorphic system. (C) Block-level schematic of the silicon neuron.

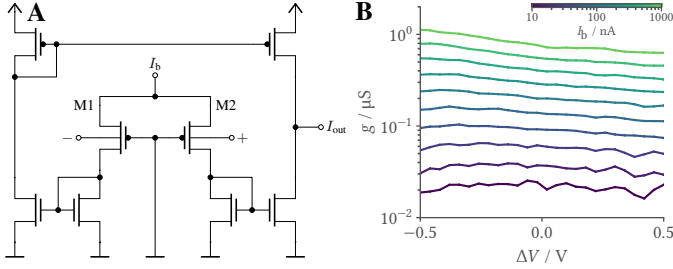


Fig. 2. (A) Bulk-driven OTA serving as a building block for the silicon neuron (simplified schematic). (B) Small signal transconductance measured for different bias currents.

mentary metal-oxide-semiconductor (CMOS) technology and occupies an active silicon area of approximately  $2575 \mu\text{m}^2$ .

### A. Bulk-driven OTA as a building block

The mostly linear nature of the differential equations behind the model dynamics emphasizes the need for an area- and energy-efficient, widely linear component, mainly to translate voltages into proportional currents. For that purpose, preceding silicon neurons have often already relied on operational transconductance amplifiers (OTAs) [6], [7]. Saturation effects and the limited linear range of standard OTA designs, however, can dramatically distort the underlying dynamics when compared to the original model equations. The presented circuits address this issue by relying on a bulk-driven differential pair (M1, M2) to linearize the characteristics of the OTA (Fig. 2 A). Bulk-driven circuits exploit the body effect to modulate a transistor’s drain current [8]. In the present case, we make use of the reduced transconductance  $g_{mb} \ll g_m$  to increase the linear input range of the OTA (Fig. 2 B), lifting the requirement for more complex and less area- or energy-efficient linearization techniques but requiring careful biasing and verification to always maintain reverse biased body diodes. Depending on the exact, application-specific dimensioning, the discussed circuit exhibits a footprint down to less than  $10 \times 10 \mu\text{m}^2$ , despite the requirement for isolated and thus spatially separated n-wells for the two transistors of the differential pair. It serves with only slight modifications to the specific instantiation as a common building block for the silicon neuron, e.g. realizing the leak conductance of the membrane dynamics (Equation (1)).

### B. Adaptation

The adaptation state variable  $w$  (Equation (2)) also resembles leaky integrator dynamics. While taking the form of a current in the model equations, it is in our silicon neuron represented as a voltage  $V_w$ . The core dynamics are, hence, implemented through a low-pass filter, directly relying on a capacitor and the bulk-driven OTA as a pseudo-conductance (Fig. 3 A), allowing to tune the adaptation time constant through its bias (Fig. 3 B). We fitted OTA2 with a second, approximately twelve-fold stronger output stage to repurpose the circuit to also generate the adaptation current  $I_w = g_w(I_b^\tau)(V_{\text{ref}} - V_w)$  directed onto the membrane.

The adaptation state is driven by the membrane-dependent subthreshold contributions on one hand and spike-triggered increments on the other. The former are realized through

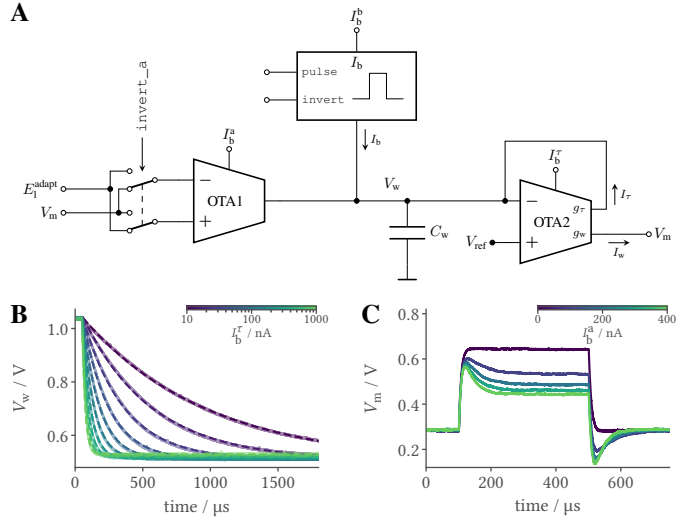


Fig. 3. (A) Schematic of the adaptation circuit. (B) Trajectory of the adaptation voltage after clamping and releasing from a fixed potential, measured for different bias currents. (C) Transient response of a membrane to a step current measured for different subthreshold adaptation strengths.

OTA1, whereby the coupling strength  $g_a(I_b^a)$  is controlled via the respective bias current (Fig. 3 C). The time-continuous dynamics of the adaptation current hence result as

$$\tau_w \frac{dI_w}{dt} = -\tau_w g_w \frac{dV_w}{dt} = \pm \underbrace{g_a(I_b^a)}_{\equiv a} \cdot (V_m - E_1^{\text{adapt}}) - I_w, \quad (4)$$

with  $\tau_w(I_b^\tau) \equiv C_w/g_\tau(I_b^\tau)$ . These dynamics are augmented by spike-triggered in- or decrements of  $V_w$  resulting from short current pulses  $I_b$  with configurable width and amplitude.

### C. Exponential feedback current

The exponential term is in its core implemented through the characteristics of a single metal-oxide-semiconductor field-effect transistor (MOSFET) biased in weak inversion (Fig. 4 A, M4). Its gate-to-source voltage is derived from the membrane via an OTA and a subsequent current-to-voltage conversion implemented straight-forwardly through a long-channeled transistor (M3) biased to operate in its linear region and thus acting as a resistor with on-resistance  $r_{\text{conv}}$ . This compact conversion circuit allows tuning the exponential current’s onset and slope (Fig. 4 B, Fig. 4 C):

$$I_{\text{exp}}(V_m) = I_0 \cdot \exp\left(\frac{8 \cdot g_{\text{ota}} \cdot [V_m - V_{\text{exp}}]}{n \cdot V_T / r_{\text{conv}}}\right). \quad (5)$$

This current is mirrored onto the membrane and can be gated either to disable the whole circuit or to “pause” the strong exponential feedback during the neuron’s refractory period. The current mirror formed by M1 and M2 rectifies the output current of OTA1 and, hence, effectively powers down the second half of the circuit for membrane potentials significantly below  $V_T$ .

### D. Emulating current- and conductance-based synapses

The synaptic integrator circuits (Fig. 5 A) represent the interface between the synapse array and the neuron’s membrane circuits. They integrate current pulses from their associated

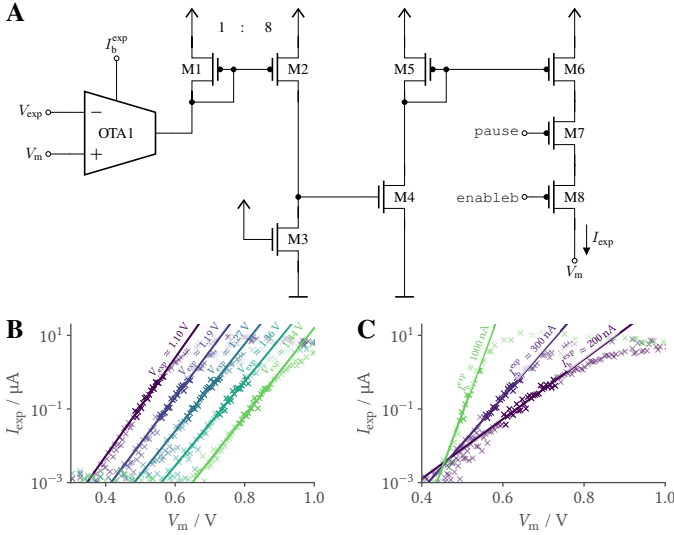


Fig. 4. (A) Exponential term. (B) & (C) The exponential current is correctly reproduced across three orders of magnitude and can be parameterized via the reference potential and the OTA’s bias. Saturation of the OTA, the current-to-voltage conversion, and the output stage limits  $I_{exp}$  but – due to the overall fast transients – does not significantly impact spike timing.

column of synapses [9] and modulate the membrane in analogy to Equation (3). Here, the low-pass filter directly exploits the synaptic line’s capacitance, which can optionally be augmented with a dedicated capacitor. The conductance (in Fig. 5 A schematically drawn as a variable resistor) is realized through multiple series-connected p-channel MOSFETs. They are biased in weak inversion to a constant gate-to-source voltage, similar to the predecessor circuit [6].

OTA1 derives a current  $I_{synin} = g_1 \cdot \Delta V_{syn}$  based on the deflection of the integrator voltage, directly implementing a *current-based* output. In that process, offsets can be compensated by tuning the voltage drop of the two source followers (M1, M2) via their bias currents. *Conductance-based* synapses (Fig. 5 B) are realized via an additional feedback path: OTA2 can modulate the bias current of OTA1 based on the membrane potential such that

$$g_1 \propto g_2 \cdot \underbrace{\left( \hat{E}_{syn} + I_b^{cuba} / g_2 - V_m \right)}_{\equiv E_{syn}}, \quad (6)$$

where  $g_1$  is assumed to be approximately proportional to the applied bias current. Mixing the static bias current with an additional, modulated component allows to create a “virtual” reversal potential  $E_{syn}$ . In the excitatory case, the latter usually extends far beyond the threshold voltage and thus falls outside the membrane’s dynamic range. Our design decouples the true zero crossing – and with it the linear range – of OTA2 from that normally never reached reversal potential.

### III. RESULTS

The neuron circuit’s dynamics can be tuned via 16 analog bias currents and 8 voltages individually provided for each neuron instance and a set of digital controls (40 bit of local static random-access memory (SRAM)) to en- or disable parts of the circuit. This large configuration space allows the flexible emulation of a wide range of model dynamics. Table I summarizes the parameter ranges achieved by the

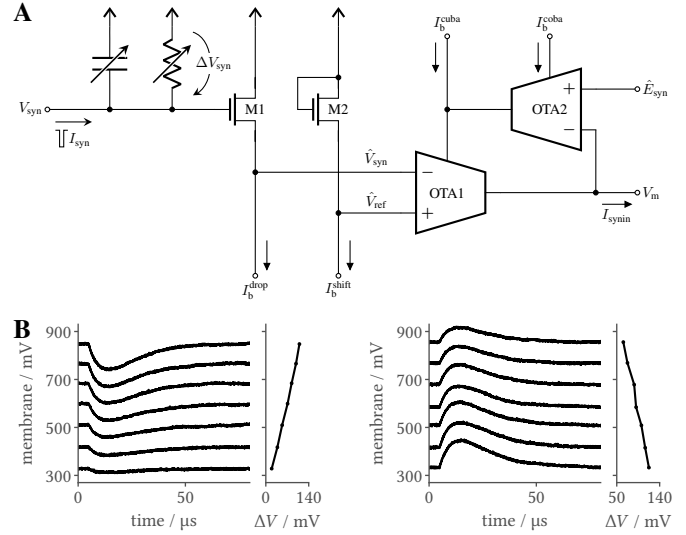


Fig. 5. (A) Simplified synaptic input circuit. (B) Postsynaptic potentials measured for various membrane potentials, implementing conductance-based synaptic interaction.

neuron design, measured across 128 neurons. The effective parameter ranges can in many cases be further extended by selecting a reduced membrane capacitance, here configured for its maximum value of approximately 2.47 pF.

With each neuron instance receiving an individual set of analog references generated by the on-chip parameter storage [10], one may not only precisely tune the operating points to certain target dynamics but can also compensate for process corner effects as well as mismatch-induced fixed-pattern variability across neurons, a process we refer to as *calibration*. The flexible parameterization and calibration allows to configure the neuron circuits for a wide range of operating points. In the following, we will demonstrate the reliability and accuracy of the silicon neuron and for that purpose, in each case, discuss the dynamics of a population of 128 calibrated neurons.

#### A. LIF neuron dynamics

Calibrating the neuron circuits to a leak-over-threshold regime exhibits well-matching dynamics (Fig. 6 A) and narrow interspike interval (ISI) distributions (Fig. 6 B). The ISIs furthermore closely correspond to those predicted by evaluating the original model equations based on the calibration targets, here measured for membrane time constants spanning two full orders of magnitude (Fig. 6 C).

A calibration of the synaptic input circuits, namely of  $\tau_{syn}$ , their effective amplitudes, and offsets, yields similarly well-

TABLE I  
PARAMETER RANGES AND VARIABILITY ACROSS 128 NEURONS.

parameter		minimum	maximum	unit
membrane time constant	$\tau_m$	$0.6 \pm 0.2$	$915 \pm 140$	$\mu s$
leak potential	$E_l$	0.0	1.0	V
firing threshold	$V_l$	0.2	1.2	V
stimulus current	$I_{stim}$	0.0	$121 \pm 14$	nA
synaptic time constant	$\tau_{syn}$	$0.29 \pm 0.03$	$538 \pm 98$	$\mu s$
synaptic peak current	$I_{syn}$	$0.033 \pm 0.003$	$1.15 \pm 0.03$	$\mu A$
adaptation time constant	$\tau_w$	$22 \pm 3$	$853 \pm 117$	$\mu s$
subthreshold adaptation	$ a $	$30 \pm 4$	$1065 \pm 114$	$\mu S$
spike-triggered adapt.	$ b $	0	$\infty$	$\mu A$
exponential slope	$\Delta_T$	$13 \pm 2$	$>91 \pm 46$	mV

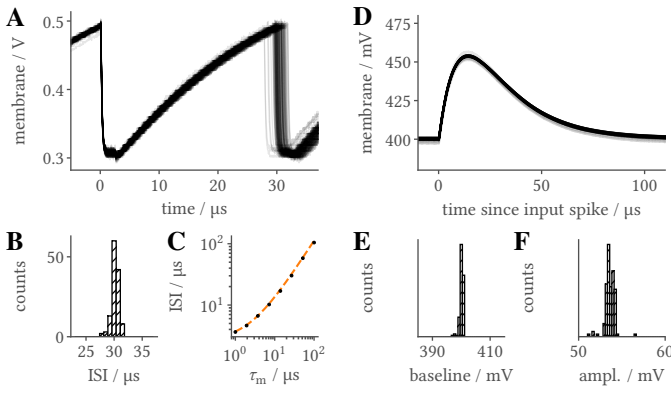


Fig. 6. (A) Traces of 128 neurons calibrated for leak-over-threshold dynamics (B) and their ISIs. (C) ISIs for different choices of  $\tau_m$  and comparison to predicted values. (D) PSP traces of 128 neurons and distributions of (E) their baselines (F) and amplitudes.

matching postsynaptic currents. This results in homogeneous postsynaptic potential (PSP) trajectories (Fig. 6D), leaving the membrane’s resting potential mostly unaffected (Fig. 6E) and yielding closely matching amplitudes (Fig. 6F).

### B. AdEx firing patterns

We benchmarked the full AdEx circuits by seeking to reproduce the different firing patterns discussed by Naud, Marcille, Clopath, *et al.* [1]. With only few exceptions, we relied on the originally published parameter sets and employed fully automated calibration routines to find suitable circuit configurations corresponding to those target dynamics. Figure 7 shows measured membrane and adaptation state traces for the first of 128 neurons. These rich dynamics all emerge as a response to a constant step current and differentiate themselves only in the neurons’ parameterizations. All calibrated 128 neurons could – with only slight deviations in the exact spike times and counts – reproduce the desired firing patterns.

## IV. DISCUSSION

The circuits discussed in this manuscript faithfully emulate the AdEx model equations and synaptic interaction. They can be precisely calibrated to a wide range of operating points and capture the model dynamics with unprecedented accuracy. Being part of the mixed-signal accelerated neuromorphic system BrainScaleS-2, they have proven themselves in a wide range of experimental studies ranging from the emulation of structured neurons to the machine-learning inspired training of spiking neural networks [11], [12].

### ACKNOWLEDGEMENTS

We thank A. Grübl, G. Kiene, Y. Stradmann, the Electronic Vision(s) group, and all others involved for their contributions.

This work has received funding from the European Union research and innovation funding H2020 945539 (HBP SGA3), DFG project EXC 2181/1 – 390900948 (STRUCTURES), the Helmholtz Association project SO-092 (ACA), and the Manfred Stärk Foundation.

### REFERENCES

- [1] R. Naud, N. Marcille, C. Clopath, *et al.*, “Firing patterns in the adaptive exponential integrate-and-fire model,” *Biological cybernetics*, vol. 99, no. 4, pp. 335–347, 2008.
- [2] J. H. Wijekoon and P. Dudek, “Integrated circuit implementation of a cortical neuron,” in *2008 IEEE International Symposium on Circuits and Systems*, IEEE, 2008, pp. 1784–1787.

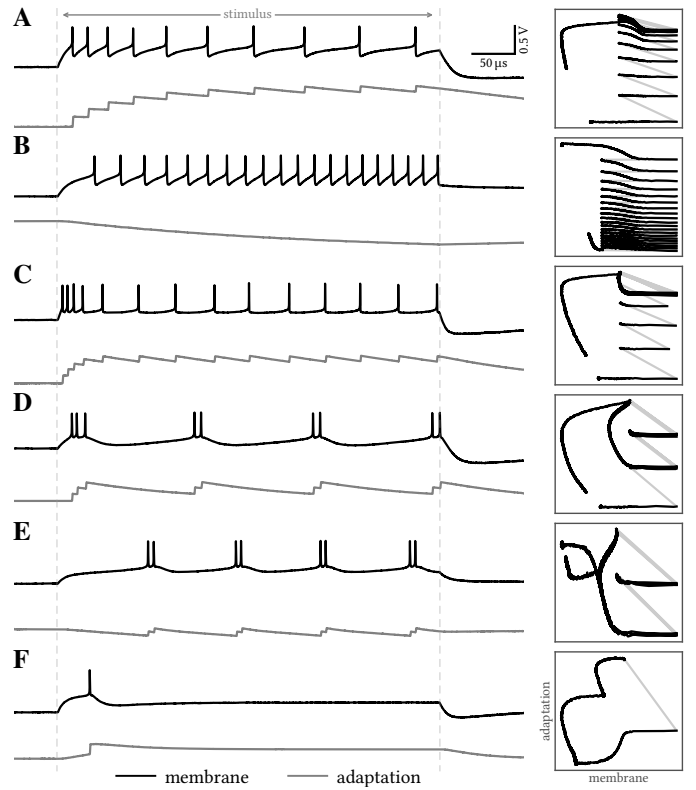


Fig. 7. Membrane and adaptation state recordings as well as the reconstructed phase plane trajectory measured for a silicon neuron parameterized for various AdEx firing patterns. (A) – (F) *Adaptation, delayed accelerating, initial burst, regular bursting, delayed regular bursting, and transient spiking.*

- [3] F. Folowosele, A. Harrison, A. Cassidy, *et al.*, “A switched capacitor implementation of the generalized linear integrate-and-fire neuron,” in *2009 IEEE International Symposium on Circuits and Systems*, IEEE, 2009, pp. 2149–2152.
- [4] A. Van Schaik, C. Jin, A. McEwan, *et al.*, “A log-domain implementation of the mihalas-niebur neuron model,” in *2010 IEEE International Symposium on Circuits and Systems*, IEEE, 2010, pp. 4249–4252.
- [5] E. Chicca, F. Stefanini, C. Bartolozzi, *et al.*, “Neuromorphic electronic circuits for building autonomous cognitive systems,” *Proceedings of the IEEE*, vol. 102, no. 9, pp. 1367–1388, 2014.
- [6] S. A. Aamir, P. Müller, G. Kiene, *et al.*, “A mixed-signal structured AdEx neuron for accelerated neuromorphic cores,” *IEEE transactions on biomedical circuits and systems*, vol. 12, no. 5, pp. 1027–1037, 2018.
- [7] S. Millner, A. Grübl, K. Meier, *et al.*, “A VLSI implementation of the adaptive exponential integrate-and-fire neuron model,” *Advances in Neural Information Processing Systems*, vol. 23, 2010.
- [8] F. Khateb, D. Birolek, N. Khatib, *et al.*, “Utilizing the bulk-driven technique in analog circuit design,” in *13th IEEE Symposium on Design and Diagnostics of Electronic Circuits and Systems*, IEEE, 2010, pp. 16–19.
- [9] S. Friedmann, J. Schemmel, A. Grübl, *et al.*, “Demonstrating hybrid learning in a flexible neuromorphic hardware system,” *IEEE transactions on biomedical circuits and systems*, vol. 11, no. 1, pp. 128–142, 2016.
- [10] M. Hock, A. Hartel, J. Schemmel, *et al.*, “An analog dynamic memory array for neuromorphic hardware,” in *2013 European Conference on Circuit Theory and Design (ECCTD)*, IEEE, 2013, pp. 1–4.
- [11] S. Billaudelle, Y. Stradmann, K. Schreiber, *et al.*, “Versatile emulation of spiking neural networks on an accelerated neuromorphic substrate,” in *2020 IEEE International Symposium on Circuits and Systems*, IEEE, 2020, pp. 1–5.
- [12] C. Pehle, S. Billaudelle, B. Cramer, *et al.*, “The BrainScaleS-2 accelerated neuromorphic system with hybrid plasticity,” *Frontiers in Neuroscience*, vol. 16, 2022, ISSN: 1662-453X. DOI: 10.3389/fnins.2022.795876.